IEEE Access
Multidisciplinary | Rapid Review | Open Access Journal

Date of publication xxxx 00, 0000, date of current version xxxx 00, 0000.

Digital Object Identifier 10.1109/ACCESS.2017.Doi Number

Leaky-Wave Antenna with Wide Scanning Range Based on Double-Layer Substrate Integrated Waveguide

PENG LUO[1], WANG HE[1], YIMING ZHANG[3], HUI LIU[1,2,3], (Member, IEEE), ERIK FORSBERG[1], (Member, IEEE), AND SAILING HE[1,2,3,4], (Fellow, IEEE)

[1]Centre for Optical and Electromagnetic Research, National Engineering Research Center for Optical Instruments, Zhejiang University, Hangzhou 310058, China
[2]Ningbo Research Institute, Zhejiang University, Ningbo 315100, China
[3]RF Circuit and Microwave System Laboratory, Centre for Optical and Electromagnetic Research, South China Academy of Advanced Optoelectronics, South China Normal University, Guangzhou 510006, China
[4]Department of Electromagnetic Engineering, School of Electrical Engineering, KTH Royal Institute of Technology, 100 44 Stockholm, Sweden

Corresponding authors: Sailing He (sailing@kth.se).

This work was supported in part by the National Key Research and Development Program of China under Grant 2018YFC1407500 and the National Natural Science Foundation of China under Grant 11621101 and Grant 61774131.

ABSTRACT A leaky-wave antenna (LWA) based on the double-layer substrate integrated waveguide (SIW) that has a wide scanning range within a narrow bandwidth is proposed. The LWA consists of two layers, each of which consists of multiple elemental SIWs arranged in parallel at each layer while the direction of the SIWs in the two layers are at an oblique angle to each other. The elemental top layer SIWs are connected to those in the bottom layer though parallelogram-shaped slots, so that the two layers together form a double-layer SIW. Thin slots etched on the upper surface of each elemental SIW of the top layer act as radiating structures. As the phase difference between the radiating slots of adjacent elemental SIWs can be enlarged by the waveguide length, wide-angle beam scanning is achieved within a specific frequency bandwidth. The proposed LWA has a scanning range from -58° to 49° in a relative bandwidth of 6.45%, from 12.75 GHz to 13.6 GHz. The scanning rate (SR), defined as the scanning range divided by the relative bandwidth, is up to 16.5. The size of structure is compact, which is $4.0\lambda_0 \times 3.6\lambda_0 \times 0.04\ \lambda_0$. The proposed LWA is suitable for radar or communication system applications.

INDEX TERMS leaky-wave antenna, beam scanning, substrate integrated waveguide, relative bandwidth, scanning rate, compact size.

I. INTRODUCTION

Leaky-wave antennas (LWAs) have in recent years gained in popularity owing to attractive characteristics such as high directivity, simple feeding architecture, and straightforward system integration ability [1]. In early works, LWAs were typically based on rectangular waveguides [2]–[5] or microstrips [6]–[8]. However, with increasing frequency, integration of rectangular waveguides and planar structures becomes progressively more difficult [9], while microstrip lines have higher loss than rectangular waveguides [10]. For these reasons, substrate integrated waveguides (SIWs) were introduced as an alternative for LWA design [12]–[17] and due to advantages such as convenient fabrication, low cost, low profile and high power capacity [18]–[19], SIW structures gained popularity [20]–[25]. In [18], the modeling, mechanisms and designs of SIWs were demonstrated.

Beam-scanning LWAs can control the beam direction, typically by changing the working frequency [1]. However, to realize a wide beam-scanning range, a large relative bandwidth is usually required. Two LWAs based on composite right/left-handed (CRLH) materials and a half mode SIW (HMSIW) with beam scanning in an angle of 130° within a relative bandwidth of 39.3% were introduced in [26], In [27], an LWA based on a microstrip spoof surface plasmon polariton transmission line able to scan from -30° to 51° within a relative bandwidth of 33.3% was demonstrated. In [28], an LWA based on S-shaped folded CSIW that had a beam scanning range from -34° to 22° within a relative bandwidth of 45.6% was proposed.

An overlarge bandwidth will impose demanding requirements on radio frequency circuitry and the available (or licensed frequency) bandwidth [23]–[24], [28]. Therefore, in certain scenarios, an LWA that can scan a wide range within a limited relative bandwidth is preferred,

This article has been accepted for publication in a future issue of this journal, but has not been fully edited. Content may change prior to final publication. Citation information: DOI 10.1109/ACCESS.2020.3035505, IEEE Access

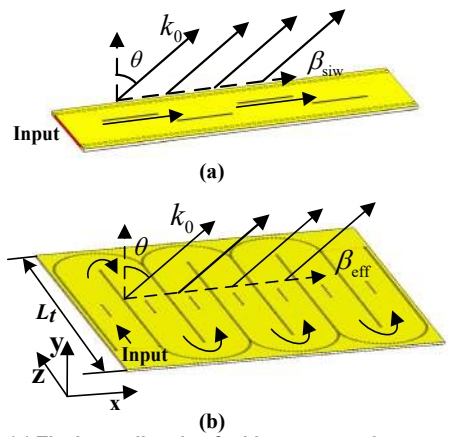

FIGURE 1. (a) The beam direction θ with respect to the normal direction of a typical straight SIW LWA, and (b) single layer SIW LWA.

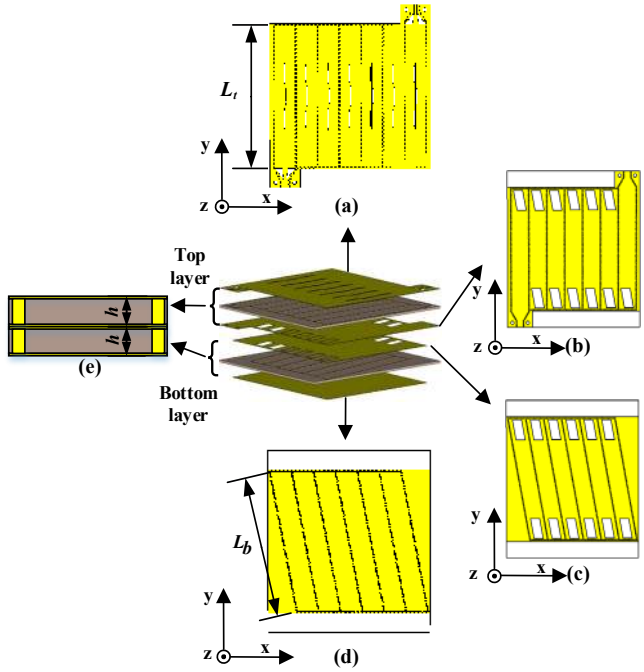

FIGURE 2. The proposed double-layer SIW-based LWA structure: (a) upper surface of the top layer, (b) lower surface of the top layer, (c) upper surface of the bottom layer, (d) lower surface of the bottom layer, and (e) side view of the LWA.

as opposed to having just a wide scanning range. In this paper, the ratio of the beam scanning range (in unit of degree) to the relative bandwidth (in unit of %), which is defined as the scanning rate (SR) [23], is used as a figure or merit.

In [23], a forward radiation LWA based on spoof surface plasmon polaritons was able to scan in an angle of 35° within a relative bandwidth of 3%, and thus had an SR of 11.7 A similar LWA with two symmetrical beams radiating simultaneous proposed in [24] has a 123° scanning range within a 9% relative bandwidth, and an SR of 13.7, which reduces gain and efficiency. In [29] , a slot array antenna based on a linearly tapered rectangular waveguide that used a spatial angular filtering metasurface achieved a scanning range of 39° with only 3.1% relative bandwidth, and an SR of 12.5.

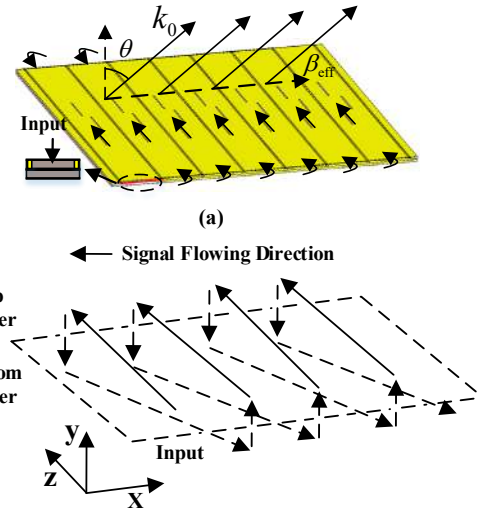

FIGURE 3. (a) The beam direction θ with respect to the normal direction of double layer SIW LWA and (b) the signal flow diagram of double layer SIW.

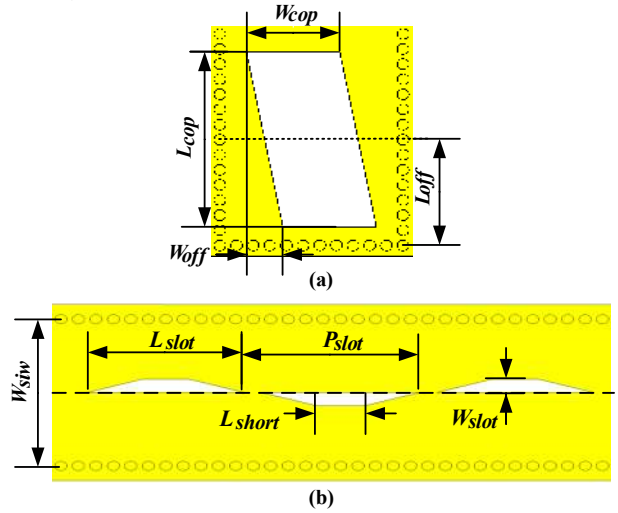

FIGURE 4. (a) The parallelogram-shaped slot and (b) the radiating slot of an elemental top layer SIW.

To achieve a larger SR, a single layer meander line structure can be used for SIW LWAs as discussed in [30]–[33]. The meander line structure can enhance the dispersion of the LWA, and thus in the same relative bandwidth, the scanning range can be enlarged. However, a meander line structure requires a large lateral size to achieve a large SR [23]–[27]. In this paper, a similar meander structure, realized with a double-layer SIW, is proposed. Compared with a single-layer structure, such a double-layer LWA enable the design of much smaller sized LWAs, higher gain and higher SR as will be shown.

This paper is organized as follows. In Section II, the structure and the principle of operation of the proposed LWA are introduced. In Section III, simulation and measurement results are analyzed. We will discuss and compare the results with other works in Section IV and the paper ends with a summary in Section V.

This article has been accepted for publication in a future issue of this journal, but has not been fully edited. Content may change prior to final publication. Citation information: DOI 10.1109/ACCESS.2020.3035505, IEEE Access

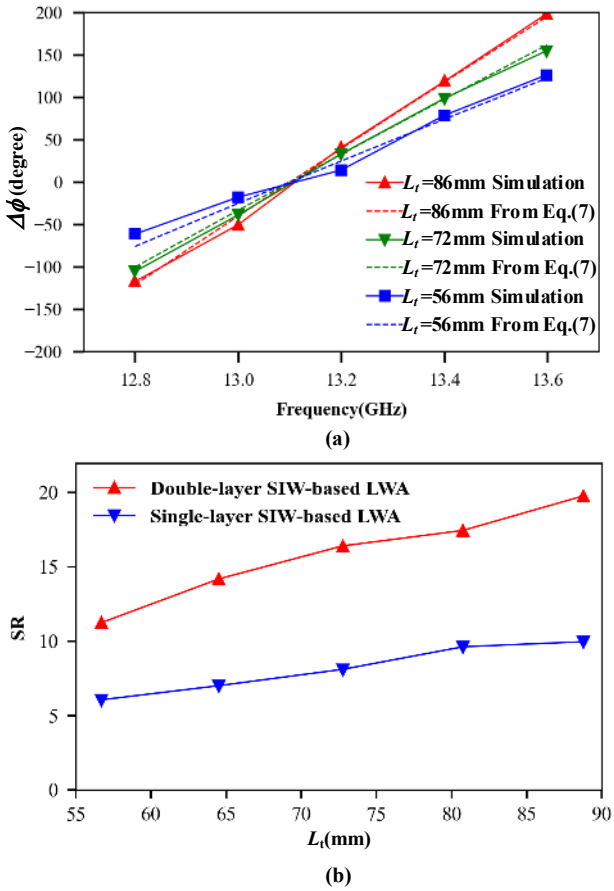

FIGURE 5. (a) $\Delta\phi$ as a function of frequency for different L_t, and (b) scanning rate as a function of L_t for the double-layer and the single-layer SIW-based LWAs.

II. STRUCTURE AND PRINCIPLE

A. STRUCTURE

For typical straight SIW LWA, as shown in Fig. 1(a), slots are etched on the SIW for radiation. The beam direction, θ, with respect to the normal direction can be calculated as [47]-[48]:

$$\theta = \arcsin\frac{\beta_{\text{eff}}}{k_0} \tag{1}$$

where k_0 is the propagation constant in free space, i.e., $k_0 = 2\pi f/c_0$, with c_0 being the speed of light in free space. β_{eff} is the effective propagation constant in waveguide. For typical straight SIW LWA, the β_{eff} is equal to β_{siw}, which for the TE_{10} mode can be expressed as:

$$\beta_{\text{siw}} = \sqrt{(2\pi f)^2\mu\varepsilon - \left(\frac{\pi}{W_s}\right)^2} \tag{2}$$

From Eq. (2), it can be concluded that the β_{siw} and the frequency changes f are positive correlated. Large relative bandwidth is need for large scanning range. The SR parameter quantifies the scanning ability, which can be calculated as:

$$SR = \frac{\theta_{\text{total}}}{B_{\text{r}}} \tag{3}$$

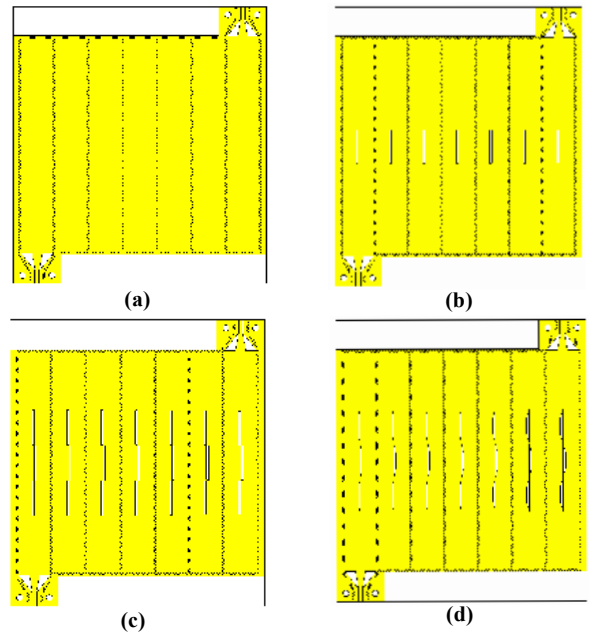

FIGURE 6. The evolutionary design process of the radiating slots of the double-layer SIW: (a) no slots, (b) a row of rectangular slots, (c) three rows of rectangular slots, and (d) three rows of slots in shape of an isosceles trapezoid.

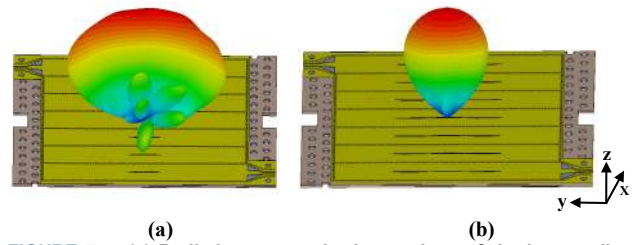

FIGURE 7. (a) Radiation pattern in the yz-plane of the intermediate design shown in Fig. 6(b) and, (b) that of the intermediate design shown Fig. 6(c).

Where θ_{total} is the total scanning range of the LWA. and B_{r} is the relative bandwidth.

To achieve a larger SR, a single layer meander line structure can be used for SIW LWAs as shown in Fig. 1(b) [30]–[33]. For such a structure, the effective propagation constant β_{eff} in x-direction can be calculated by:

$$\beta_{\text{eff}} = \frac{\Delta\phi}{W_s} \tag{4}$$

Where $\Delta\phi$ is the phase difference between the adjacent elemental SIWs, and W_s is the width of the elemental SIW. For the single layer meandering waveguide, $\Delta\phi^S$ can be expressed as:

$$\Delta\phi^S = \beta_{\text{siw}}(L_t + L_e) \tag{5}$$

Where L_t is the length of the SIWs as shown in Fig. 1(b). L_e is the equivalent length of the meander structure between adjacent SIWs. Thus the effective propagation constant of single layer β_{eff}^S can be approximated by:

$$\beta_{\text{eff}}^S = \frac{(L_t + L_e)}{W_s}\cdot\sqrt{(2\pi f)^2\mu\varepsilon - \left(\frac{\pi}{W_s}\right)^2} \tag{6}$$

This article has been accepted for publication in a future issue of this journal, but has not been fully edited. Content may change prior to final publication. Citation information: DOI 10.1109/ACCESS.2020.3035505, IEEE Access

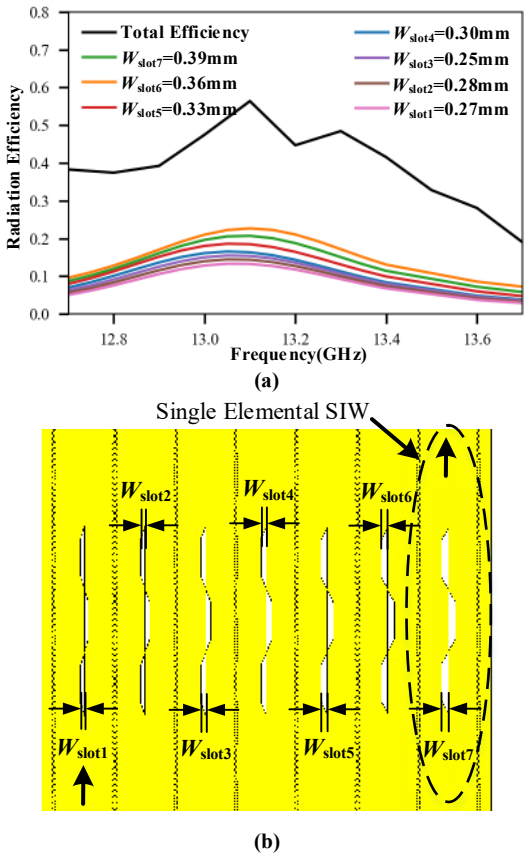

FIGURE 8. **(a) Radiation efficiency of the three radiating slots over a single elemental SIW with different slot widths, W_{slot}, and the total efficiency (black curve) of the LWA. (b) The widths of the three radiating slots on different elemental SIWs.**

Compare the Eq. (6) with Eq. (2), it is clear that the variation of β_{siw} increases when the frequency changes in same relative bandwidth. Smaller relative bandwidth is required to acquire the same scanning range for single layer SIW LWA.

For higher SR and compact size, we use coupling structure to replace meander line structure and adopt double layer SIW structure to realize the LWA.

A schematic of the proposed LWA design is shown in Fig. 2. It consists of two Taconic TLY-5 substrate layers [11], with a permittivity of 2.2 and a thickness of 0.508 mm, one stacked on top of the other as shown in Fig 2(e). Both layers consist of multiple elemental SIWs arranged in parallel. In the top layer, the SIWs are aligned parallel to the y-direction, while in the bottom layer, the SIWs are arranged at an oblique angle relative to the SIWs in the top layer. The lower surface of the top layer is arranged in close contact with the upper surface of the bottom layer. Through parallelogram shaped slots between the two layers, shown in Fig. 2(b) and Fig.2(c), the elemental top layer SIWs are sequentially coupled to the bottom layer SIWs constructing a single meandering double-layer SIW. Fig. 4(a) details the dimensions of the coupling slots between the two layers. Transition structures from the SIW to grounded coplanar waveguides (GCPW) are included at the two ends of the double-layer SIW [34]. The total size

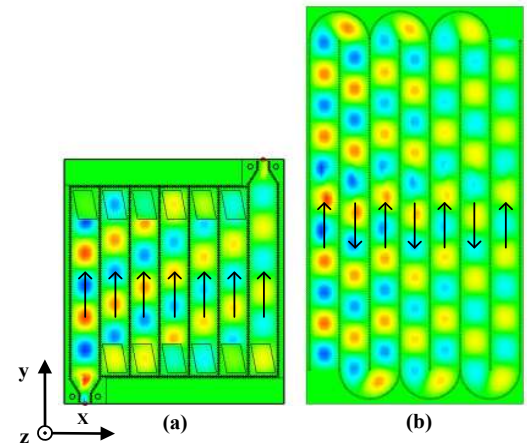

FIGURE 9. **The electric field distributions in (a) the double-layer SIW-based LWA and (b) an equivalent conventional single-layer SIW-based LWA. The arrows denote the propagation direction.**

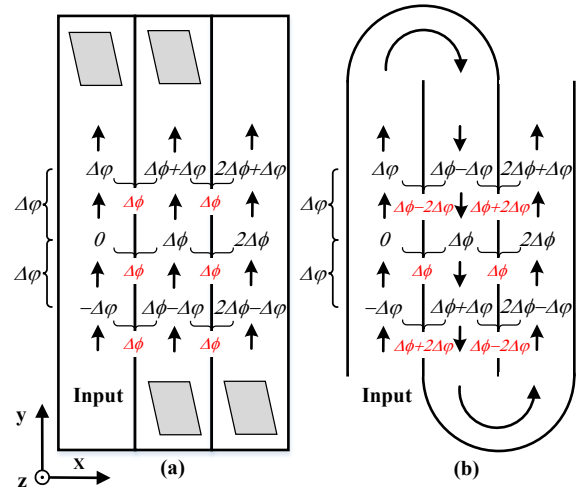

FIGURE 10. **The phase differences of the adjacent radiating slots in *x*-direction for (a) the double-layer SIW-based LWA and (b) the conventional single-layer SIW-based LWA. $\Delta\varphi$ is the phase difference of adjacent slots in *y*-direction.**

of the structure is $4.0\lambda_0 \times 3.6\lambda_0 \times 0.04\ \lambda_0$, where λ_0 is the center frequency free space wavelength (13.15 GHz). The beam direction θ, with respect to the normal direction for double layer SIW LWA is shown in Fig. 3(a). The signal flow diagram is shown in Fig. 3(b)

For the double layer meandering waveguide, $\Delta\phi^D$ can be expressed as:

$$\Delta\phi^D = \beta_{\mathrm{siw}}(L_{\mathrm{t}} + L_{\mathrm{b}} + 2L_{\mathrm{e}}) \tag{7}$$

L_t and L_b are the length of the top-layer SIWs and the bottom-layer SIWs, respectively as shown in Fig. 2. L_e is the equivalent length of the coupling slots between the two layers. Since $L_t \approx L_b$, β_{eff}^D can be approximated by:

$$\beta_{\mathrm{eff}}^D \approx \frac{2(L_t + L_e)}{W_s}\sqrt{(2\pi f)^2 \mu\varepsilon - \left(\frac{\pi}{W_s}\right)^2} \tag{8}$$

By inspection of Eq. (8) it is clear that, given a fixed bandwidth $[f_1, f_2]$, the range of β_{eff}, $[\beta_{\mathrm{eff},2}, \beta_{\mathrm{eff},1}]$, can be enlarged by increasing L_t and it is about 2 times bigger than

This article has been accepted for publication in a future issue of this journal, but has not been fully edited. Content may change prior to final publication. Citation information: DOI 10.1109/ACCESS.2020.3035505, IEEE Access

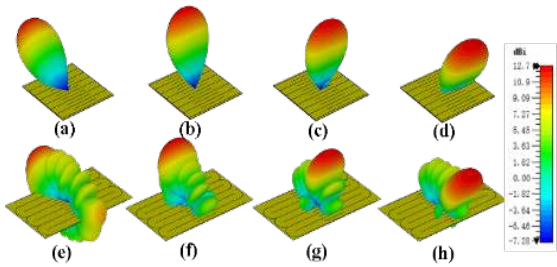

FIGURE 11. Simulated radiation patterns of the double-layer SIW-based LWA at (a) 12.8 GHz, (b) 13.1 GHz, (c) 13.3 GHz, and (d) 13.5 GHz and the single-layer SIW-based LWA at (e) 12.6GHz, (f) 12.8GHz, (g) 13.1GHz, and (h) 13.3GHz.

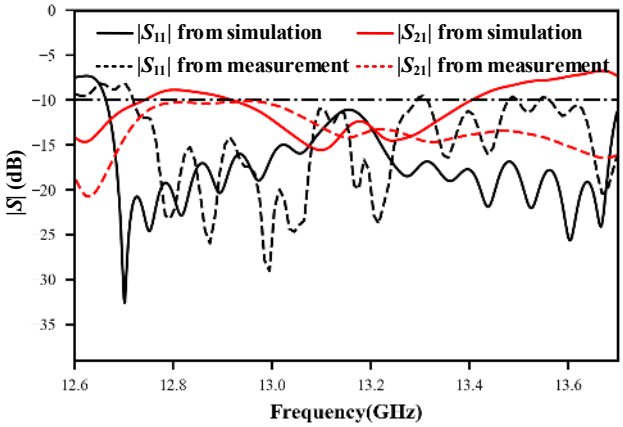

FIGURE 12. Simulated and measured |S| parameters of the double-layer LWA.

single layer structure compared with Eq.(6). I.e. double layer structure LWA has much larger SR than single layer structure.

Fig. 5(a) shows $\Delta\phi$ as a function of frequency for different L_t. Solid lines are derived from simulations, and dashed lines are calculated using Eq. (7), and we can see that the simulation and analytical results agree well. Within the considered relative bandwidth, $\Delta\phi$ increases from negative to positive as the frequency increases, indicating that the LWA can scan the beam from backward to forward. The slopes of the curves increases, and hence the dispersion is enhanced, with larger L_t. Fig. 5(b) shows the SR dependence on L_t for both single-layer and double-layer SIW-based LWAs, and it can be seen that the SR can be also enhanced with by increasing L_t. In addition, with the same L_t, the SR of the double-layer structure is obviously larger than that of the single-layer structure. Double layer structure is better chose to realized high SR LWA, and the SR could be adjusted by the length.

B. RADIATION

To enable radiation, slots are etched on the upper surface of the elemental top layer SIWs, the dimensions of which (over a single elemental SIW) are depicted in Fig. 4(b). The slot design evolution is shown in Fig. 6. Fig. 6(a) shows the double-layer SIW without any slots on the outer surfaces. As a first design iteration, a single row of rectangular slots is added to the upper surface in the middle of the element SIWs, as shown in Fig. 6(b). With changing frequency, the radiation from these slots can achieve beam scanning in the *xz*-plane.

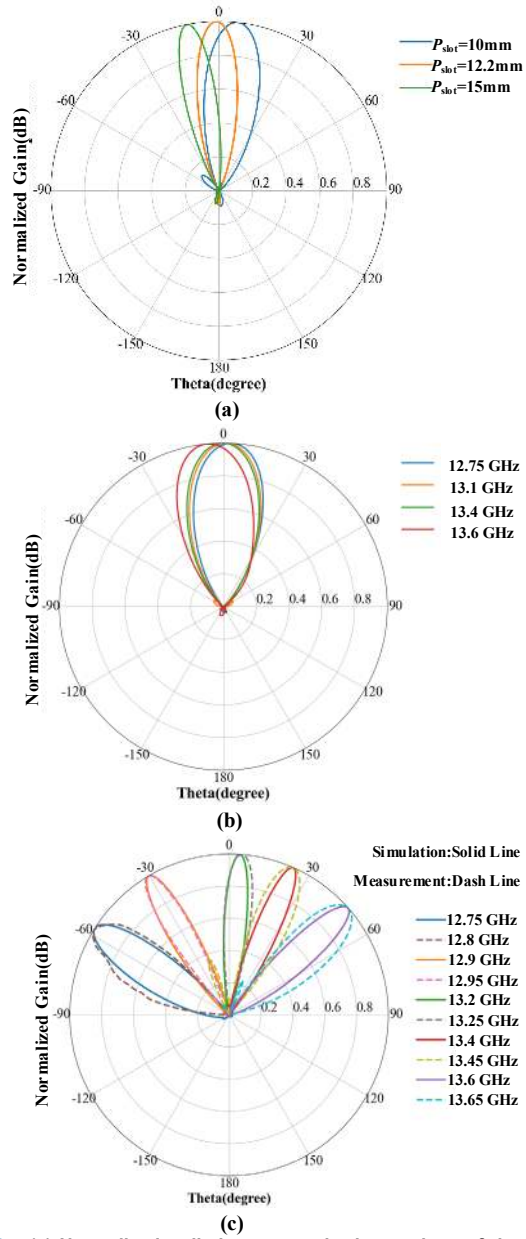

FIGURE 13. (a) Normalized radiation pattern in the *yz*-plane of three slots on a single SIW at center frequency. (b) Normalized radiation pattern in the *yz*-plane and (c) simulated and measured radiation patterns of the double-layer LWA in the *xz*-plane.

To compress the beamwidth in the *y*-direction and increase the antenna gain, two additional rows of slots are added as shown in Fig. 6(c). The upper-row slots and the lower-row slots are offset from the middle-row slots in the *x*-direction like the references [35]–[37]. To optimize the design, the rectangular slots are reshaped into isosceles trapezoids, Fig 6(d), as such tapering helps to reduce the wave reflection in the waveguide at the location of the slots and improve reflection coefficient of the LWA.

For comparison we plot in Fig. 7 the radiation patterns in the yz-plane for the evolutionary designs in Fig. 6(b) and Fig. 6(c). It is clear that the beamwidth in y-direction is compressed and the gain is enhanced.

This article has been accepted for publication in a future issue of this journal, but has not been fully edited. Content may change prior to final publication. Citation information: DOI 10.1109/ACCESS.2020.3035505, IEEE Access

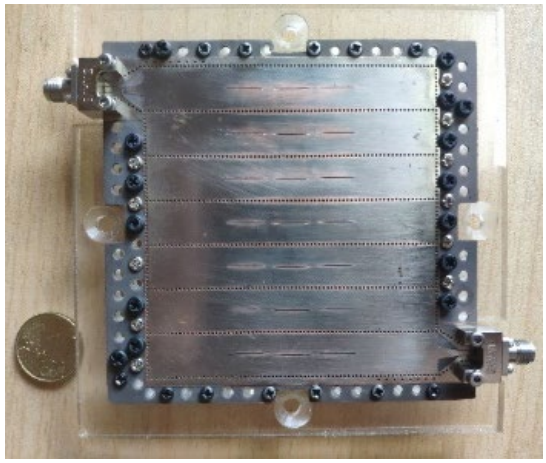

FIGURE 14. **The fabricated LWA.**

The radiation efficiency [38] of one single radiating slot can be adjusted by changing its width. As the radiation occurs at each slot, the energy of the propagating wave in the SIW decreases gradually. To ensure that the power leaking out from the slots distribute evenly across the LWA, the width of the slots is designed in such a way that it increases as the distance between the slot and the feeding port increases [50], as shown in Fig. 8(b). For design simplicity, we choose the width of the slots in the same radiating elemental SIW to be the same. The radiation efficiency of the three radiating slots in a single elemental SIW in the upper layer is plotted in Fig. 8(a), which clearly shows that with increasing slot width, more power is radiated from the slots. The total radiation efficiency, i.e. the sum from the seven radiating elemental SIWs, is plotted as the black line in Fig. 8(a). There is a drop at center frequency because of the reflection. At the frequency of center, the distance in same y-axis value between the adjacent SIWs is integral multiple wavelength. Which is easy to form standing wave and result in the deterioration of the S11.

C. DESIGN STEPS

The selection of the initial geometrical parameters and the subsequent design steps for the LWA could were the following:

The width of the SIW, W_{siw}, is first calculated with respect to the bandwidth. As we require only the TE10 mode to be present, the cut-off frequency of the SIW must be less than the minimum frequency of the bandwidth, and the cut-off frequency must be two times greater than the maximum bandwidth. We then calculate the length of the LWA, L_{t}, using Eqs. (1) and (7) and the required SR. The length of the parallelogram coupling slots L_{cop} is about half the wavelength, and the width W_{cop} of the parallelogram coupling slots is about half the width of the SIW.

The number of slots on one elemental SIW can be decided by the length of the SIW, L_{t}, and he period of the slots, P_{slot}. As shown in Fig. 13(a), at center frequency the direction of the array is affected by the slot period, P_{slot}, and, if we want the radiation pattern be vertical to the xy-plane, the period of the slots should be about half the center frequency wavelength

TABLE 1. **Geometrical parameters of the structure (unit: mm)**

Symbol	Value	Symbol	Value
W_{siw}	11	L_{short}	5.06
W_{cop}	5.61	P_{slot}	11.45
L_{t}	73.5	L_{b}	74.8
h	0.508	L_{cop}	11.6
L_{slot}	11.26	L_{off}	6.76
W_{slot1}	0.25	W_{off}	2.2
W_{slot3}	0.28	W_{slot2}	0.27
W_{slot5}	0.33	W_{slot4}	0.30
W_{slot7}	0.39	W_{slot6}	0.36

The number of radiating elementa SIWs can be estimated by the required directivity as the directivity increases with increasing number of elemental SIWs. We can treat the slots on the same elemental SIW in the y-direction as one radiating element and calculate the number of required radiating elemental SIWs as outlined by Balanis [50]. The sidelobe level is determined by the power distribution and here we adopt a uniform linear power distribution. Triangular or sinusoidal distributions can also be used for special requirements of sidelobe levels or directivity [50]. The width of the elemental SIWs is estimated by the required power proportion.

Following initial design as described above, all the parameters can be further optimized by the CST software.

D. COMPARISON

To demonstrate the advantage of the double-layer design, we compare with a conventional single-layer SIW LWA. To maintain the same dispersion, the length of the single-layer SIW is twice that of the double-layer SIW. As can be seen in Fig. 9, the electric field distributions in the top layer of the double-layer SIW are compared with those of the single-layer SIW. For the double-layer SIW, the directions of the mode propagation in all elemental SIWs in the top layer are the same, while for the single-layer SIW, the directions of the mode propagation in the adjacent elemental SIWs are opposing. Fig. 10 shows the phase at the positions of the radiating slots as well as the phase difference of the adjacent slots in the x-direction. For the double-layer SIW, the phase difference between the adjacent slots in the x-direction are the same for each slot row, i.e., $\Delta\phi$. For the single-layer SIW, only the middle row of the radiating slots has a fixed phase difference in x-direction, and the phase difference of the upper and lower slot rows alters between $\Delta\phi - 2\Delta\varphi$ and $\Delta\phi + 2\Delta\varphi$, where $\Delta\varphi$ is the phase difference between adjacent slots in y-direction. The different phase distributions of the double-layer and single-layer SIWs will lead to different radiation patterns, and simulations of these at

This article has been accepted for publication in a future issue of this journal, but has not been fully edited. Content may change prior to final publication. Citation information: DOI 10.1109/ACCESS.2020.3035505, IEEE Access

TABLE 2. Performance comparison of SIW-based LWAs

	Center frequency (GHz)	Scanning range (degree)	Relative bandwidth (%)	Size (λ_0)	Gain (dBi)	Scanning Rate
[39]	11	60	16.4	10.26*0.4	12-13	3.7
[30]	25.25	50	9.9	9.62*7.6*0.5	11.1-14.4	5.1
[49]	11.4	124	24.5	5.7*1	16.2-18	5.1
[51]	5.6	107	18	4.62*0.54	8.33-12.3	5.9
[31]	24	60	8.3	7.14*6.0	8.9-11.7	7.2
[52]	60	120	16.67	5.6	14.5	7.2
[40]	9.6	39	3.1	10.56*0.5	12-15	12.6
[24]	11.1	123	9	7.4*0.5	7.3–9.6	13.7
This paper	**13.18**	**107**	**6.45**	**4.0*3.6**	**9.6-14.3**	**16.5**

different frequencies are shown in Fig. 11. At each frequency, the radiation pattern of the single-layer structure has more side lobes than the double-layer structure. The amount of side lobes for the single-layer structure can be reduced by only using the middle-row slots, however at the expense of a widened beamwidth in the *y*-direction and a reduced gain. In comparison, the double-layer structure allows for multiple rows of slots that compress the beamwidth and enhance the gain without introducing side lobes.

III. SIMULATION AND MEASUREMENT RESULTS

The parameter values for the final LWA design are listed in Table I. Fig. 14 shows the fabricated LWA. The principal aim of this paper is proof-of-concept of a method to design a high-SR LWA, and for this reason we have opted for a frequency range lower than that used for common millimeter wave radar applications to reduce fabrication complexity. The method is equally applicable for longer wavelengths/lower frequencies. To fix the two layers, via holes are arranged and machine screws are used around the edge of the substrate.

Simulated and measured $|S_{11}|$ of the LWA are shown in Fig. 12 The $|S_{11}|$ measurement is done using an Agilent N5247A vector network analyzer. The $|S_{11}|$ -10 dB bandwidth ranges from about 12.7 GHz to about 13.6 GHz for both simulations and measurements. Due to some minor fabrication imperfections, some small frequency shift between the simulations and measurements can be seen. In addition, as the via holes used to fix the two layers can only be located around the LWA edges, there exist a tiny air gap between the two layers at the location of the coupling slots, which will affect the coupling between the SIWs of the two layers thus distort $|S_{11}|$ somewhat.

Simulated and measured radiation patterns are shown in Fig. 13(c), and we can see that they agree well. The minor difference in frequency at the same radiation angle between simulations and measurement may again be attributed to fabrication errors. When the beam scans from -58° to 49°, the corresponding frequencies range from 12.8 GHz to 13.65 GHz. Therefore, the total scanning angle is 107°, corresponding to a relative bandwidth of 6.42%, and thus the SR is 16.6. The max measured realized gains during the bandwidth is 12.5dBi.

Since a single element SIW on the top layer will in itself act as a small LWA along the *y*-direction, as the frequency changes, the beam will scan in *yz*-plane. However, in a narrow bandwidth, the range in which β_{siw} can vary is limited compared to that of β_{eff} and therefore, the beam scanning in *yz*-plane should be negligible compared with that in *xz*-plane. Fig. 13(b) shows the normalized radiation pattern cuts in the *yz*-plane at four frequencies. Within the considered bandwidth, the beam scans from -6° to 4° in *yz*-plane, with a total scanning angle of only 10°. In contrast, the total scanning angle in *xz*-plane is much larger than 10°.

IV. DISCUSSION

A comparison of the LWA proposed in this paper with previous works is shown in Table II.

First, due to the double-layer meandering SIW structure, the LWA proposed here has the highest SR among the listed works.

Second, we should furthermore note that the SR can be further increased by increasing L_t, as shown in Fig. 5(b) for conventional meandering single-layer SIW-based LWA [30]–[31], but the resulting size will be much larger than that of a double-layer SIW structure with the same SR. The LWA proposed have the smallest size while have highest SR.

Additionally, due to the fixed phase difference in the *x*-direction between the adjacent elemental SIWs in the top layer, multiple rows of radiating slots can be arranged on the double-layer LWA without generating side lobes, and thus it is easier for the double-layer LWA to achieve higher gains than a conventional single-layer LWA. Noted that, the LWA proposed in [31] has simulated gains varying from 8.9dBi to 11.7dBi, which are smaller than the simulated gains from 9.6dBi to 14.3dBi in this work. To enhance the gain of the single-layer LWA, a phase-correcting grating (PCG) cover is adopted in [30], through which the gain is enhanced up to 14.4dBi, but an extra height of half wavelength is required to add the PCG cover.

For future work, the LWA with high SR proposed in this

paper may be developed into an LWA working at a single frequency with a varactor diode or liquid crystals to enable electrical control of the beam scanning. Varactor diodes [41]–[42] and liquid crystals [43]–[44] have been utilized to control the beam-scanning angle of LWAs at a fixed frequencies. However, due to the limited dynamic range of varactor diodes and liquid crystals as well as low SR, the scanning range of these LWAs are limited to about 15°–45° [43]–[46]. In contrast, by using the LWA with high SR presented in this work, the scanning range of an electrically tunable LWA may be further enhanced.

V. CONCLUSION

We have proposed and analyzed an LWA with high SR based on a double-layer SIW. The beam scanning angle ranges from -58° to +49° within a bandwidth from 12.75 GHz to 13.6 GHz with a relative bandwidth of 6.45% and the SR is 16.5. As compared to conventional single-layer SIW-based LWAs, by using multiple rows of radiating slots, a higher gain is achieved and the radiation pattern display a much smaller amount of side lobes. Additionally, the double-layer LWA is smaller in size. The advantage of using limited relative bandwidth to scan the beam in a wide angle makes the LWA attractive for radar applications or in communication systems.

REFERENCES

[1] D. R. Jackson, C. Caloz and T. Itoh, "Leaky-wave antennas," *Proc. IEEE*, vol. 100, no. 7, pp. 2194-2206, 2012.

[2] C. Damm, M. Maasch, R. Gonzalo and R. Jakoby, "Tunable composite right/left-handed leaky wave antenna based on a rectangular waveguide using liquid crystals", in *Proc. IEEE MTT-S International Microwave Symposium*, 2010, pp. 13-16.

[3] R. D. Seager and J. C. Vardaxoglou, "Characterisation of leaky wave antennas constructed from solid rectangular waveguides with a dipole frequency selective surface sidewall", in *Proc. IEE National Conference on Antennas and Propagation.*, 1999, pp. 295-298.

[4] P. Pan, F. Meng and Q. Wu, "A composed right/left-handed waveguide with open-ended corrugations for backward-to-forward leaky-wave antenna application," *Microw. Opt. Techn. Let.*, vol. 50, no. 3, pp. 579-582, 2008.

[5] L. Goldstone and A. Oliner, "Leaky-wave antennas I: rectangular waveguides," *IEEE Trans. Antennas Propag.*, vol. 7, no. 4, pp. 307-319, 1959.

[6] C. Hu, C. F. Jsu and J. Wu, "An aperture-coupled linear microstrip leaky-wave antenna array with two-dimensional dual-beam scanning capability," *IEEE Trans. Antennas Propag.*, vol. 48, no. 6, pp. 909-913, 2000.

[7] C. Wang, C. F. Jou and I. Chen, "Electronically switchable beam patterns using leaky-wave antenna", in *Proc. IEEE Antennas and Propagation Society International Symposium*, 2001, pp. 780-783.

[8] D. A. Tonn and R. Bansal, "Travelling wave microstrip dipole antennas," *Electron. Lett.*, vol. 31, no. 24, pp. 2064-2066, 1995.

[9] D. Deslandes and K. Wu, "Integrated microstrip and rectangular waveguide in planar form," *IEEE Microw. Compon. Lett.,* vol. 11, no. 2, pp. 68-70, 2001.

[10] D. M. Pozar, "Microwave engineering," 3rd ed., Hoboken, N.J: J. Wiley, 2005, pp. 169-173.

[11] Advanced PCB Materials Product Selection Guide. US. [Online]. Available:https://www.4taconic.com/uploads/ADD%20Data%20Sheets/1558470066_selector%20guide%20global.pdf, July 18th, 2020.

[12] R. Noumi, J. Machac, N. Boulajefan and A. Gharsallah, "Development of SIW LWA from non-uniform CRLH unit cells with SLL reduction," *Mediterranean Microwave Symposium (MMS)*, 2018, pp. 146-148.

[13] D. K. Karmokar, Y.J. Guo, P. Qin, S. Chen and T.S. Bird, "Substrate integrated waveguide-based periodic backward-to-forward scanning leaky-wave antenna with low cross-polarization," *IEEE Trans. Antennas Propag.*, vol. 66, no. 8, pp. 3846-3856, 2018.

[14] Y. Lyu, F. Meng, G. Yang, D. Erni, Q. Wu and K. Wu, "Periodic SIW leaky-wave antenna with large circularly polarized beam scanning range," *IEEE Antennas Wireless Propag. Lett.*, vol. 16, pp. 2493-2496, 2017.

[15] J. Machac, M. Polivka and K. Zemlyakov, "A dual band leaky wave antenna on a CRLH substrate integrated waveguide," *IEEE Trans. Antennas Propag.*, vol. 61, no. 7, pp. 3876-3879, 2013.

[16] A. J. Martinez-Ros, J. L. Gómez-Tornero and G. Goussetis, "Multifunctional angular bandpass filter SIW leaky-wave antenna," *IEEE Antennas Wireless Propag. Lett.*, vol. 16, pp. 936-939, 2017.

[17] N. Gupta and V. D. Kumar, "Transverse bow-tie slotted substrate integrated waveguide leaky-wave antenna", in *Proc. Annual IEEE India Conference (INDICON)*, 2013, pp. 1-4.

[18] D. Deslandes and K. Wu, "Accurate modeling, wave mechanisms, and design considerations of a substrate integrated waveguide," *IEEE Trans. Microw. Theory Techn.*, vol. 54, no. 6, pp. 2516-2526, 2006.

[19] Y. Cassivi, L. Perregrini, P. Arcioni, M. Bressan, K. Wu and G. Conciauro, "Dispersion characteristics of substrate integrated rectangular waveguide," *IEEE Microw. Compon. Lett.,* vol. 12, no. 9, pp. 333-335, 2002.

[20] J. Liu, W. Zhou and Y. Long, "A simple technique for open-stopband suppression in periodic leaky-wave antennas using two nonidentical elements per unit cell," *IEEE Trans. Antennas Propag.*, vol. 66, no. 6, pp. 2741-2751, 2018.

[21] Y. Lyu, *et al*., "Leaky-wave antennas based on noncutoff substrate integrated waveguide supporting beam scanning from backward to forward," *IEEE Trans. Antennas Propag.*, vol. 64, no. 6, pp. 2155-2164, 2016.

[22] Y. Lyu, F. Meng, G. Yang, D. Erni, Q. Wu and K. Wu, "Periodic SIW leaky-wave antenna with large circularly polarized beam scanning range," *IEEE Antennas Wireless Propag. Lett.*, vol. 16, pp. 2493-2496, 2017.

[23] D. Guan, Q. Zhang, P. You, Z. Yang, Y. Zhou and S. Yong, "Scanning rate enhancement of leaky-wave antennas using slow-wave substrate integrated waveguide structure," *IEEE Trans. Antennas Propag.*, vol. 66, no. 7, pp. 3747-3751, 2018.

[24] S. Xu, *et al*., "A wide-angle narrowband leaky-wave antenna based on substrate integrated waveguide-spoof surface plasmon polariton structure," *IEEE Antennas Wireless Propag. Lett.*, vol. 18, no. 7, pp. 1386-1389, 2019.

[25] Z. Wang and C. Park, "Novel substrate integrated waveguide (SIW) type high power amplifier using microstrip-to-SIW transition", in *Proc. Asia-Pacific Microwave Conference Proceedings (APMC)*, 2013, pp. 101-103.

[26] Y. Dong and T. Itoh, "Composite right/left-handed substrate integrated waveguide and half mode substrate integrated waveguide leaky-wave structures," *IEEE Trans. Antennas Propag.*, vol. 59, no. 3, pp. 767-775, 2011.

[27] D. Wei, J. Li, J. Yang, Y. Qi and G. Yang, "Wide-scanning-angle leaky-wave array antenna based on microstrip SSPPs-TL," *IEEE Antennas Wireless Propag. Lett.*, vol. 17, no. 8, pp. 1566-1570, 2018.

[28] Y. Zhang, H. Liu, C. Meng, Y. Lin, Y. Zhang, E. Forsberg, and S. He, "A Novel Millimeter-Wave Backward to Forward Scanning Periodic Leaky-Wave Antenna Based on Two Different Radiator Types," Progress In Electromagnetics Research, Vol. 168, 31-38, 2020.

[29] A. Zhang, R. Yang, D. Li, B. Hu, Z. Lei and Y. Jiao, "Metasurface-based tapered waveguide slot array antennas for wide angular scanning in a narrow frequency band," *IEEE Trans. Antennas Propag.*, vol. 66, no. 8, pp. 4052-4059, 2018.

[30] W. Cao, W. Hong, Z. N. Chen, B. Zhang and A. Liu, "Gain enhancement of beam scanning substrate integrated waveguide slot array antennas using a phase-correcting grating cover," *IEEE Trans. Antennas Propag.*, vol. 62, no. 9, pp. 4584-4591, 2014.

[31] L. Chiu, W. Hong and Z. Kuai, "Substrate integrated waveguide slot array antenna with enhanced scanning range for automotive application", in *Proc. Microwave Conf. Asia Pacific.,* 2009, pp. 1-4.

[32] A. Shoykhetbrod, D. Nussler and A. Hommes, "Design of a SIW meander antenna for 60 GHz applications", in *Proc. German Microwave Conference*, 2012, pp. 1-3.
[33] B. Li, H. Zhong, W. Ma, W. Cao and X. Yang, "A circularly polarized substrate integrated waveguide slot array antenna with enhanced scanning range", in *Proc. International Conference on Microwave and Millimeter Wave Technology (ICMMT)*, 2019, pp. 1-3.
[34] R. Kazemi, A. E. Fathy, S. Yang and R. A. Sadeghzadeh, "Development of an ultra wide band GCPW to SIW transition," *IEEE Radio and Wireless Symposium*, 2012, pp. 171-174.
[35] S. Liao, P. Chen, P. Wu, K. M. Shum and Q. Xue, "Substrate-integrated waveguide-based 60-ghz resonant slotted waveguide arrays with wide impedance bandwidth and high gain," *IEEE Trans. Antennas Propagat.*, vol. 63, no. 7, pp. 2922-2931, 2015.
[36] G. A. Casula and G. Montisci, "Design of Dielectric-Covered Planar Arrays of Longitudinal Slots," *IEEE Antennas Wireless Propag. Lett.*, vol. 8, pp. 752-755, 2009.
[37] G. Mahmoudi, H. Oraizi, K. Malekzadeh and M. T. Noghani, "Design, optimization and VSWR improvement of a standing wave longitudinal slot array on a rectangular waveguide", in *Proc. Iranian Conference on Electrical Engineering*, 2011, pp. 1-5.
[38] Y. Geng, J. Wang, Y. Li, Z. Li, M. Chen and Z. Zhang, "High-efficiency leaky-wave antenna array with sidelobe suppression and multibeam generation," *IEEE Antennas Wireless Propag. Lett.*, vol. 16, pp. 2787-2790, 2017.
[39] J. Liu, X. Tang, Y. Li and Y. Long, "Substrate integrated waveguide leaky-wave antenna with H-shaped slots," *IEEE Trans. Antennas Propag.*, vol. 60, no. 8, pp. 3962-3967, 2012.
[40] A. Zhang, R. Yang, D. Li, B. Hu, Z. Lei and Y. Jiao, "Metasurface-based tapered waveguide slot array antennas for wide angular scanning in a narrow frequency band," *IEEE Trans. Antennas Propag.*, vol. 66, no. 8, pp. 4052-4059, 2018.
[41] K. Chen, Y. H. Zhang, S. Y. He, H. T. Chen and G. Q. Zhu, "An electronically controlled leaky-wave antenna based on corrugated siw structure with fixed-frequency beam scanning," *IEEE Antennas Wireless Propag. Lett.*, vol. 18, no. 3, pp. 551-555, 2019.
[42] D. K. Karmokar, K. P. Esselle and S. G. Hay, "Fixed-frequency beam steering of microstrip leaky-wave antennas using binary switches," *IEEE Trans. Antennas Propag.*, vol. 64, no. 6, pp. 2146-2154, 2016.
[43] S. Ma, *et al*., "Beam scanning range expansion of liquid crystal based leaky wave antennas", in *Proc. IEEE International Symposium on Electromagnetic Compatibility and IEEE Asia-Pacific Symposium on Electromagnetic Compatibility (EMC/APEMC)*, 2018, pp. 1123-1125.
[44] C. Damm, M. Maasch, R. Gonzalo and R. Jakoby, "Tunable composite right/left-handed leaky wave antenna based on a rectangular waveguide using liquid crystals", in *Proc. IEEE MTT-S International Microwave Symposium.*, 2010, pp. 13-16.
[45] B. Che, F. Meng, J. Fu, K. Zhang, G. Yang and Q. Wu, "A dual band CRLH leaky wave antenna with electrically steerable beam based on liquid crystals", in *Proc. IEEE Conference on Electromagnetic Field Computation (CEFC)*, 2016, pp. 1.
[46] M. Roig, M. Maasch, C. Damm and R. Jakoby, "Dynamic beam steering properties of an electrically tuned liquid crystal based CRLH leaky wave antenna", in *Proc. International Congress on Advanced Electromagnetic Materials in Microwaves and Optics*, 2014, pp. 253-255.
[47] F. XuK. Wu and X. Zhang, "Periodic Leaky-Wave Antenna for Millimeter Wave Applications Based on Substrate Integrated Waveguide," IEEE T. Antenn. Propag., vol. 58, no. 2, pp. 340-347, 2010.
[48] D.R. Jackson and A.A. Oliner, "Modern Antenna Handbook,", 1st ed., New York, NY, USA:Wiley, 2008, pp. 325-367.
[49] A. Sarkar, A. Sharma, A. Biswas and M.J. Akhtar, "Communication Compact CRLH Leaky-wave Antenna using TE20 Mode Substrate Integrated Waveguide for Broad Space Radiation Coverage," IEEE T. Antenn. Propag. pp. 1, 2020.
[50] C.A. Balanis, "Antenna theory: analysis and design,", 3rd ed., Hoboken, NJ: Wiley-Interscience, 2005.
[51] D.K. Karmokar, Y.J. Guo, S. Chen and T.S. Bird, "Composite Right/Left-Handed Leaky-Wave Antennas for Wide-Angle Beam Scanning With Flexibly Chosen Frequency Range," IEEE T. Antenn. Propag., vol. 68, no. 1, pp. 100-110, 2020.
[52] A. Sarkar and S. Lim, "60 GHz Compact Larger Beam Scanning Range PCB Leaky-Wave Antenna Using HMSIW for Millimeter-Wave Applications," IEEE T. Antenn. Propag., vol. 68, no. 8, pp. 5816-5826, 2020.

Peng Luo received the B.E. degree in electronic information science and technology from Southwest Jiaotong University, Sichuan, China, in 2018. He is currently pursuing the M.S. degree with the Centre for Optical and Electromagnetic Research, Zhejiang University, Hangzhou, China. His current research interests include antenna design and leaky-wave antennas.

Wang He received the B.E. degree in information engineering and the Ph. D degree in optical engineering from Zhejiang University, Hangzhou, Zhejiang, China, in 2015 and 2020, respectively. His current research interests include electromagnetics and antenna design.

Yiming Zhang was born in Xianyang, China. He received the B.S. degree in electronic science and technology from the Shaanxi University of Science and Technology, Xi'an, China, in 2016. He is currently pursuing the M.S. degree in electromagnetic field and microwave technology with the Centre for Optical and Electromagnetic Research, South China Academy of Advanced Optoelectronics, South China Normal University, Guangzhou, China. His current research interests include microwave components, RF circuits, RFID antennas, mm-wave antennas, and arrays.

Hui Liu (Member, IEEE) was born in Zhumadian, China. He received the M.S. degree in electromagnetic field and microwave technology from South China Normal University, China, in 2013, and the Ph.D. degree in microelectronics and solid state electronics from the Centre for Optical and Electromagnetic Research, Academy of Advanced Optoelectronics, South China Normal University, in 2018. He was a Post-Doctoral Researcher with the Center for Optical and Electromagnetic Research, Zhejiang University between 2018 and 2020. He joined the School of Electronic and Information at Guangdong Polytechnic Normal University as a faculty member in 2020. His research interests include antenna, RF circuits and microwave components.

Erik Forsberg (Member, IEEE) received the M.S. degree in engineering physics and the Ph.D. degree in photonics from the Royal Institute of Technology (KTH), Sweden, in 1996 and 2003, respectively. He also studied business and economics at the Stockholm School of Economics, Sweden. In 2000, he was a Visiting Scientist with Hokkaido University, Japan, and a Postdoctoral Fellow with KTH, in 2003. He was a Faculty Member with Zhejiang University (ZJU), China, from 2004 to 2008. From 2009 until 2012, he was the Founding Graduate Dean (associate) with the Higher Colleges of Technology (HCT), United Arab Emirates. In 2013, he rejoined ZJU as an Associate Professor. His current research interests include nano-lasers, plasmonics and optical fiber devices.

This article has been accepted for publication in a future issue of this journal, but has not been fully edited. Content may change prior to final publication. Citation information: DOI 10.1109/ACCESS.2020.3035505, IEEE Access

Sailing He (Fellow, IEEE) received the Licentiate of Technology and the Ph.D. degree in electromagnetic theory from the Royal Institute of Technology (KTH), Stockholm, Sweden, in 1991 and 1992, respectively. Since then he has worked in the same devision of the Royal Institute of Technology as an Assistant Professor, an Associate Professor, and a Full Professor. He is also with Zhejiang University as a distinguished professor, as well as the director for a joint research center (JORCEP) between KTH and ZJU. His current research interests include applied electromagnetics, optoelectronics, and sensing applications. He has first-authored one monograph and authored/coauthored about 600 papers in refereed international journals. Prof. He is a Fellow of IEEE, Optical Society of America (OSA), the International Society for Optical Engineering (SPIE) and the Electromagnetics Academy